Journal of Power Sources 186 (2009) 89–95

Contents lists available at ScienceDirect

Journal of Power Sources

journal homepage: www.elsevier.com/locate/jpowsour

Temperature and performance variations along single chamber solid oxide fuel cells

Bertrand Morel[a,1], Réal Roberge[b,*], Sylvio Savoie[b], Teko W. Napporn[a], Michel Meunier[a]

[a] Département de Génie Physique, Ecole Polytechnique de Montréal, Québec H3C 3A7, Canada
[b] Institut de recherche d'Hydro-Québec (IREQ), Varennes, Québec J3X 1S1, Canada

ARTICLE INFO

Article history:
Received 28 July 2008
Received in revised form
15 September 2008
Accepted 19 September 2008
Available online 2 October 2008

Keywords:
Single chamber solid oxide fuel cells (SC-SOFCs)
Electrochemical impedance spectroscopy (EIS)
Combustion
Temperature gradients
Gas distribution
Performance

ABSTRACT

The catalytic activity of single chamber solid oxide fuel cells (SC-SOFCs) with respect to hydrocarbon fuels induces a major overheating of the fuel cell, temperature variations along its length, and changes in the original fuel/air composition mainly over the anode component. This paper assesses the temperature gradients and the variations in performance along electrolyte-supported Ni-YSZ/YSZ/LSM cells fed with methane gas. The investigations are performed in a useful range of CH_4/O_2 ratios between 1.0 and 2.0, in which the furnace temperature and flow rate of methane–air mixtures are held constant at 700 °C and 450 sccm, respectively. Electrochemical impedance spectroscopy (EIS) is used to sense the temperature at the location where smaller size cathodes are positioned on the opposite side of a full-size anode. Due to temperature increases, cells always perform better when the small cathodes are located at the inlet as well as at a CH_4/O_2 ratio of 1.0. With an increase in ratio, the results show the presence of artefacts due to the use of an active LSM material for the combustion of methane, and open-type gas distribution plates for the single chamber reactor.

1. Introduction

Single chamber solid oxide fuel cells (SC-SOFCs) operate in direct contact with hydrocarbon–air mixtures. Their proper functioning is generally dependent on the heterogeneous catalysis of the feeding hydrocarbon species at the anode and the high selectivity of the cathode for the electroreduction of oxygen [1–7]. Such distinct properties of the cell components are at the origin of the high open circuit voltage (OCV) values normally observed. Indeed, extremely low $p(O_2)_a$ builds up at the anode/electrolyte interface due to the combustion of the incoming fuel while the $p(O_2)_c$ at the cathode remains fairly high with the use of materials inert to hydrocarbon combustion. However, deviations from such ideal behaviour have been found, especially when the cathode side becomes susceptible to combustion reactions. This has been verified, for example, in the case of perovskite oxide materials, the morphology and structure of which have not been properly optimized for the single chamber application or for which the fuel cells are operated at too high temperatures [8–11]. This generally leads to decreases in OCV and fuel cell performance.

The catalytic activity of the electrode materials also generates large amounts of heat, which leads to the establishment of a true cell temperature that differs significantly from the temperature settings of the furnace [9,12–15]. According to the fuel cell types, its electrode materials and the hydrocarbon fuel used, the heat released by the combustion reactions may increase the cell temperature from about 20 to 250 °C [10,12,13]. Such overheating could be considered as an SC-SOFCs advantage. Indeed, Shao et al. [16] demonstrated the operation of a micro-SOFCs stack at 500–600 °C in the absence of any external heating.

More recently, we measured the overheating as well as the temperature gradient along single chamber electrolyte-supported cells exposed to a CH_4/O_2 ratio of 1.0 at 700 °C [17]. This was done by realizing electrochemical impedance spectroscopy (EIS) spectra of cells made of small cathodes located at the inlet, center, and outlet of larger electrolyte-supported cells, with the small cathodes facing a full-size anode on the other side. The temperature at the inlet rose by more than 100 °C while a fall of as much as 50 °C was recorded within the first cm length of the fuel cell. Concurrently, this fall in temperature from the cell inlet to its outlet forces a performance gradient largely governed by the

* Corresponding author. Tel.: +1 514 652 8172; fax: +1 514 652 8625.
E-mail address: roberge.real@ireq.ca (R. Roberge).
[1] Present address: CEA-Grenoble, 38054 Grenoble cedex 09, France.

0378-7753/$ – see front matter © 2008 Elsevier B.V. All rights reserved.
doi:10.1016/j.jpowsour.2008.09.087

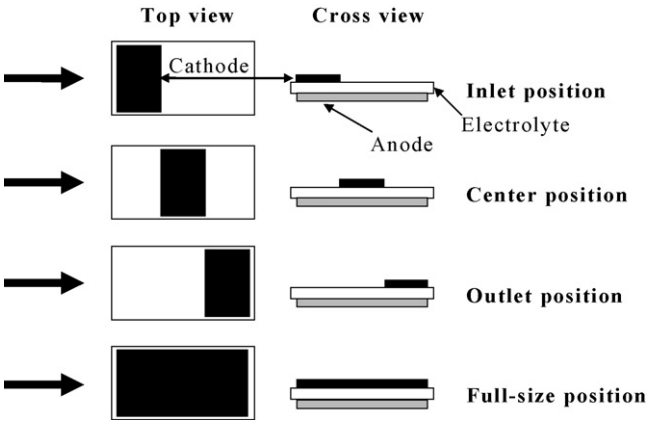

Fig. 1. Schematic diagram of the different cathode geometries tested with a full-size anode surface area on the opposite side.

resistance of the thick electrolyte that is also a function of temperature.

Temperature variations along the cells are not the only factor impacting the performance of SC-SOFCs. Indeed, the combustion processes found at the cell inlet are also expected to play a major role. In the case of partial oxidation reactions, for example, the methane combustion leads to the enrichment of H_2 and CO gas species. As shown before [11], modifications of the chemical environment over the anode component lead to increases in the fuel-to-oxygen ratios at the cell outlet compared to the original incoming CH_4/O_2 ratio. The variation in the outlet fuel-to-oxygen ratio is dependent on the true combustion mechanism as well as the CH_4/O_2 ratio. This last parameter has also been shown to significantly affect the performance of SC-SOFCs and to be practical only in a limited range of the methane-to-oxygen ratio [15,18–21].

In the present paper, we are thus continuing our investigation of single chamber Ni-YSZ/YSZ/LSM fuel cells fed by various incoming mixtures of methane and oxygen gas. We are extending our previous results on overheating, the temperature gradient and the variations in performance in SC-SOFCs [17] by performing extensive measurements in a useful range of CH_4/O_2 ratios between 1.0 and 2.0. The results are discussed in terms of temperature and environmental changes caused by the combustion reactions in the single chamber reactor.

2. Experimental

Detailed descriptions of the experimental parameters have been published elsewhere [11,17]. Only a brief account will be given here. Electrolyte-supported cells are made of 500-μm-thick 8YSZ membranes. The electrodes are composed of two layers. The anodes are essentially made of 45 wt% NiO/55 wt% YSZ to which a thin NiO layer is added as electrical contact. The cathodes are formed from an internal functional layer of 50 wt% $La_{0.8}Sr_{0.2}MnO_3$ (LSM)/50 wt% YSZ to which a pure LSM layer is added for improved conductivity. Final sintering of the anode and cathode layers is performed for 3 h at 1375 and 1100 °C, respectively.

The electrolyte membrane measures 16 mm × 25 mm. As depicted in Fig. 1, smaller size cathodes ($S = 1.07\ cm^2$) placed alongside the electrolyte-supported cells and full-size cathodes ($S = 3.2\ cm^2$) are used. The small cathode cells were used to evaluate the effect of both the temperature and the environmental changes along the SC-SOFCs. In the following section, all the results are normalized against the corresponding geometric cathode areas.

The cells are tested in an experimental setup (Fig. 2a) similar to the one described earlier [3]. Minor changes have been made since then especially in relation to the gas distribution plates (GDP) that support the cells and the current collectors (gold meshes). Fig. 2b and c shows 3D views of the plates used in the present study. They are made of alumina and contain evenly spaced posts that uniformly mix the gas over the electrodes. The plates in Fig. 2a were already used in our previous paper [17] and continue to serve here for comparing cell performance at each CH_4/O_2 ratio. As can be seen, they are of an open design with posts up to the sides. A closed design (Fig. 2c) was also used during the study to clarify some unusual results obtained with the small cathode cell in the outlet. In this case, solid walls form the sides and the outlet face of

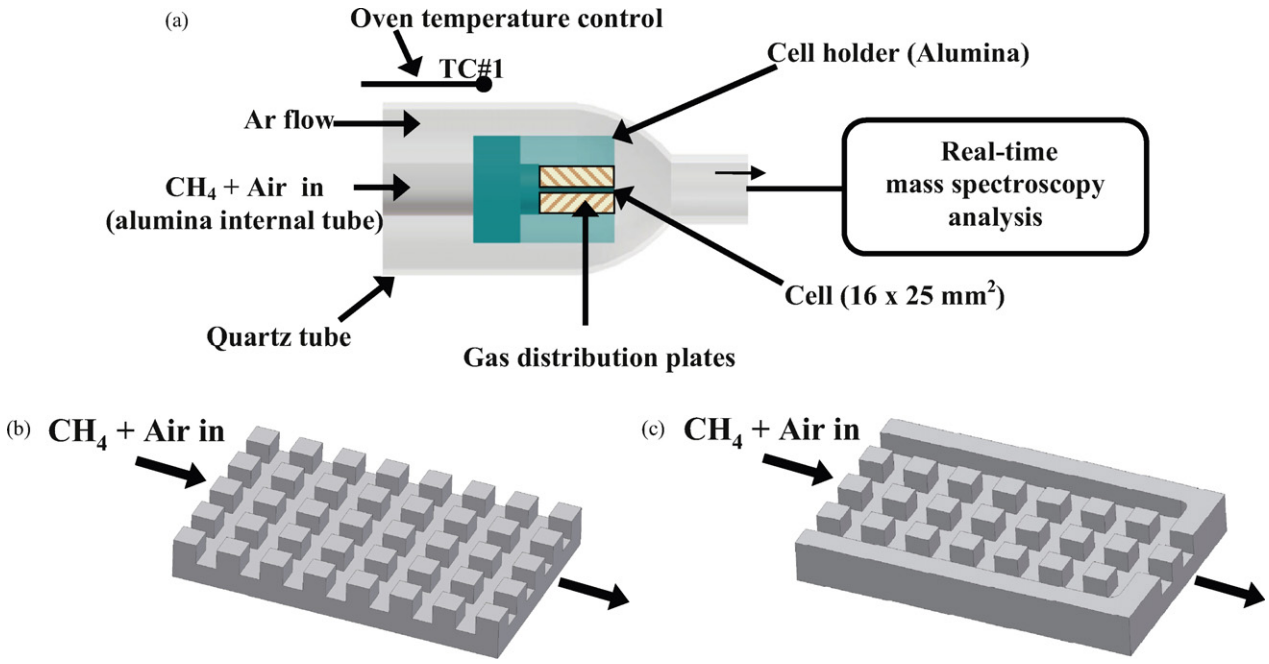

Fig. 2. (a) Schematic of the single chamber setup used for testing the 16 mm × 25 mm electrolyte-supported cells; (b and c) 3D views of open and closed gas distribution plates, respectively.

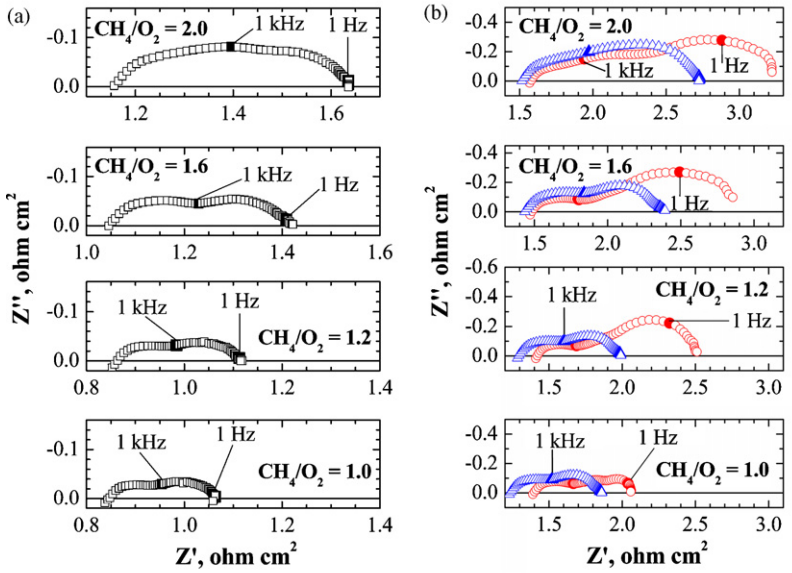

Fig. 3. Impedance spectra of Ni-YSZ/YSZ/LSM cells measured at OCV and 700 °C against various CH_4/O_2 ratios. (a) Small LSM cathode located at the cell inlet and (b) small LSM cathodes located at the center (△) and outlet (○). Experiments performed in an open GDP reactor. The 1 Hz and 1 kHz data points are marked with filled symbols.

the plates except for two holes that allow the gas species to flow out and the connecting experimental wires to pass through. The entire assembly of distribution plates, current collectors and cells is firmly held in place inside the cell holder (Fig. 2a) and forms the so-called single chamber fuel cell split into an anode and a cathode reactor.

Before testing under the various ratios of CH_4/O_2 = 1.0, 1.2, 1.6 and 2.0, the cells were heated at a nominal temperature of 700 °C and reduced in an argon/methane mixture. Experiments were performed at 700 °C under a total flow rate of 450 sccm CH_4 and synthetic air (80:20 Ar/5%He:O_2). Current–voltage curves (Solartron 1286) and impedance measurements (Solartron SI 1260) were carried out in a two-electrode 4-wire configuration. Frequencies were varied from 100 kHz to 0.1 Hz.

3. Results and discussion

3.1. EIS as a function of cathode positioning and CH_4/O_2 ratio

Fig. 3 first shows the EIS spectra of the small cathode cells located at the inlet, center and outlet position of the electrolyte-supported half-cell anodes. Table 1 compares their low and high frequency intercept values which are related under our experimental conditions to electrolyte resistance (R_{HF}) and total cell resistance ($R_{t,cell}$), respectively. On thick electrolyte cells, R_{HF} may be used to evaluate the real cell temperature at the specified cathode location and the temperature gradient that follows the combustion reactions.

Table 1
Characteristic EIS values of R_{HF} and $R_{t,cell}$ as a function of the CH_4/O_2 ratio measured at OCV on small cathode cells located at the inlet, center, and outlet, of identical electrolyte-supported half-cell anodes and for a full-size cathode.

CH_4/O_2	R_{HF} (Ω cm²)				$R_{t,cell}$ (Ω cm²)			
	Inlet	Center	Outlet	Full-size	Inlet	Center	Outlet	Full-size
2.0	1.16	1.52	1.58	1.77	1.64	2.74	3.34	2.85
1.6	1.05	1.44	1.48	1.75	1.42	2.40	2.95	2.59
1.2	0.86	1.29	1.42	1.49	1.12	1.99	2.51	2.10
1.0	0.85	1.24	1.40	1.33	1.07	1.86	2.06	1.84

Experiments performed in an open GDP reactor at 700 °C and 450 sccm total flow rate.

This was shown before at CH_4/O_2 = 1.0 using independent measurements of the ionic conductivity of the 8YSZ electrolyte (E_a = 0.81 eV and σ_o = 297 S cm^{-1}) [17]. It will be extended here in a range of useful CH_4/O_2 ratios up to 2.0.

3.1.1. Temperature rise and gradient

A comparison of the EIS spectra at the cell inlet (Fig. 3a) and at the center and outlet positions (Fig. 3b) shows R_{HF} values consistently lower at the cell inlet than anywhere else along its length. As expected, larger elevations of temperature occur at the very far end of the fuel inlet due to the fast combustion processes that are taking place in presence of the fresh methane and oxygen gas mixture. Moreover, an increase in CH_4/O_2 also causes an increase in the R_{HF} value. At the inlet, for example, R_{HF} increases from 0.85 to 1.16 Ω cm² from CH_4/O_2 = 1.0 to 2.0. The parallel increase in temperature at the lowest CH_4/O_2 ratios has to be accounted for by a reaction mechanism pathway at the anode that favours the more exothermic reactions in the event that the oxygen content of the incoming gas is increased. Nickel is indeed poorly selective and both the partial and complete oxidation reactions have been found under single chamber conditions [16,22]. When the small cathodes are located at the center and the outlet position of the cells, the R_{HF} values are much closer to each other even more so as the CH_4/O_2 ratios reach 1.6 and 2.0. The temperature rise trends from the outlet to the inlet and from CH_4/O_2 = 2.0 to 1.0 are shown in Fig. 4. Under our conditions, the maximum increase in cell temperature is observed at the inlet and for CH_4/O_2 = 1.0. At that location, a ΔT_{calc} of 135 °C is found between the cell and the furnace. Downstream, the increase in temperature drops sharply to about 90 °C at the center and then more slowly down to 75 °C at the outlet. Similar behaviours are found at other CH_4/O_2 ratios.

The above increases in temperature are impressive. Nevertheless, they still represent only the average values measured by EIS at the location of the small 1 cm² cathodes. In reality, however, even more important rises are expected locally. In fact, the presence of hot spots such as those found in fixed-bed reactors for the partial oxidation of methane to synthesis gas [23] may certainly not be ignored, at least at the fuel cell inlet. Although such overheating in SC-SOFCs is well-known, the present work and [17] demonstrate for the first time that the sustained combustion of the hydrocarbon

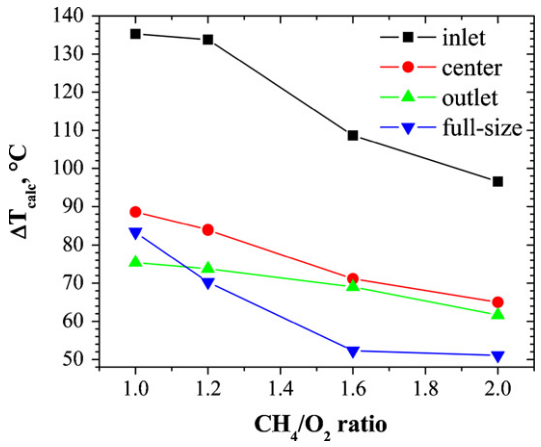

Fig. 4. Temperature rise calculated from the high-frequency resistance (R_{HF}) measured by EIS on a full-size Ni-YSZ/YSZ/LSM cell as well as on small cathode electrodes located at the inlet, center, and outlet of identical electrolyte-supported half-cell anodes. Experiments performed in an open GDP reactor at 700 °C and 450 sccm total flow rate.

fuel gives rise to marked exothermic heating effects at the cell inlet, as well as to inhomogeneous temperature distributions and steep temperature gradients along the length of the fuel cell. Such effects have been simply neglected before in SC-SOFCs owing to the small surface areas ($\leq$1 cm^2) of the cells used in the laboratory experiments. However, one has to be aware of their possible contributions to the early degradation and failure of SC-SOFCs, especially with the use of higher hydrocarbon fuels that liberate even larger quantities of reaction heat.

3.1.2. Low frequency semicircles at the outlet cathode cell

The difference in temperature due to the combustion of methane at the different CH_4/O_2 ratios not only affects R_{HF} but also the total cell resistance $R_{t,cell}$. Complying with the decrease in cell temperatures, both resistances increase with an increase in CH_4/O_2 and from the inlet to the outlet (Table 1). This expected behaviour is, however, accompanied at the outlet by an additional feature in the EIS spectra. As shown in Fig. 3b, an extra semicircle characterized by a summit frequency of about 1 Hz is indeed rapidly expanding at low frequency from CH_4/O_2 = 1.0 to 2.0. On the basis of cell temperature alone, such behaviour is difficult to understand. At CH_4/O_2 ratios of 1.6 and 2.0, for example, overheating at the outlet and the center position differs by less than 5 °C (Fig. 4). Such a small difference can hardly justify the presence of LF impedance at the outlet cathode only. Moreover, our previous studies on LSM symmetrical cells showed the possibility of oxygen depletion and low frequency semicircles [11]. However, these phenomena were observed only in cases where the complete oxidation reaction of CH_4 and the associated temperature were at their maximum. Conversely, here, the outlet cathode is always the coldest of the three positions.

In the absence of any direct temperature effect to account for the presence of the LF semicircles at the outlet cathode cell, the possible changes in the gas phase chemistry downstream of the fuel cell inlet have to be considered. Indeed, the fact of moving the third of a full-size cathode along an electrolyte-supported anode would be similar to measuring the EIS spectra of a complete cell exposed to the environment and the temperature found at this particular location. On the cathode side, we assume that the environment first seen at each of the three locations is the actual CH_4/O_2 gas mixture entering the single chamber. Indeed, it was previously shown that our conditions did not favour the catalytic oxidation of methane on YSZ [3,13]. When in contact with the cathode, the environment is rapidly modified by the complete oxidation reactions forming CO_2 and H_2O. However, these reactions are less favoured at the outlet since cell temperatures are at their lowest there. The chemistry that occurs on the cathode side can thus hardly explain the presence of the low frequency semicircle. On the anode side, the gas species are expected to rapidly change from the initial CH_4/O_2 mixture at the inlet to a complex environment formed of the unconverted CH_4 and O_2 species and of the combustion reaction products (H_2, CO, CO_2 and H_2O) in the direction of the outlet [17]. The H_2 and to a lesser extent the CO species should be more electrochemically active than the methane species on the Ni-YSZ cermet. Easier reaction processes would thus be expected at the anode sites that face a cathode positioned at the outlet of the cell, which negates the occurrence of an LF semicircle.

Factors other than the normal change in cell temperature and gas phase composition must intervene to explain the LF impedance at the most downstream position. The LF semicircles are observed in the setup that uses the open GDP shown in Fig. 2b. To explain their presence, the assumption is that rapid and major changes occur in the flow of the gas species going downstream over the electrodes. Although the plates were designed to evenly distribute the incoming fuel mixture and the formed reaction products over the electrodes, they obviously do not constrain the gas inside the reactors. More precisely, sudden combustion, temperature rise and volume expansion occur at the cell inlet and downstream. This is followed by fast heat and mass transfer inside the reactors that results in significant increases in the gas leakage from the sides of the distribution plates and into the cell holder. This enhanced lateral flow rate affects both sides of the cells. However, the observed increase in the impedance of the outlet cathode cell with a decrease into the O_2 content of the incoming fuel mixture, i.e., with an increase in CH_4/O_2, suggests that the process is controlled by the oxygen gas species of the cathodic reactor. It may thus be compared to an oxygen depletion process.

To verify the above hypotheses, we tested a second small cathode cell at the outlet but which was this time contained within a reactor made of the closed GDP shown in Fig. 2c. Such a design is more restrictive since the only leakage from the sides would come from the unsealed current collectors pressed between the plates and the electrodes. EIS spectra from the second outlet cathode cell were recorded under the same experimental conditions as with the more open plate design. The plots obtained for these identical cells are compared in Fig. 5. At every CH_4/O_2 ratio, similar spectra are recorded except for the LF semicircles, which either disappear or become small enough to be buried under the other impedance features for the cell contained between closed gas distribution plates. More experiments would probably be required to confirm our hypothesis of accelerated lateral flow rates and oxygen depletion in the cathodic reactor; however, the actual results with two different gas distribution plates already raise the question of proper flow design under single chamber SOFC conditions. As will be shown later, induced oxygen depletion in the cathode reactor also leads to lower OCV values for the small cathode cell when positioned at the outlet.

3.2. EIS of a complete cell (full-size cathode) as a function of the CH_4/O_2 ratio

The EIS spectra of the complete cell made of a full-size cathode are shown in Fig. 6. Their characteristic values of R_{HF} and $R_{t,cell}$ may be compared with the individual cases above in Table 1. As expected, the R_{HF} value of the full-size cathode increases with the CH_4/O_2 ratio due to a decrease in mean cell temperature. However, it also becomes significantly higher than even the R_{HF} value for the cathode positioned at the outlet, and it levels off at CH_4/O_2 = 2.0. As shown in Fig. 4, ΔT_{calc} calculated using the impedance spectra

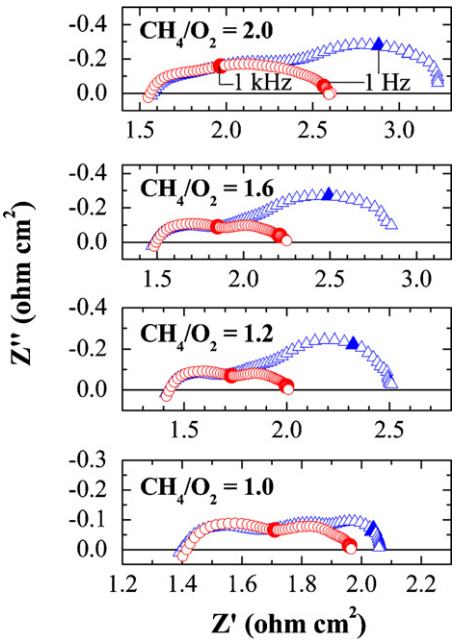

Fig. 5. Impedance spectra of the Ni-YSZ/YSZ/"small-outlet-located LSM" cells in (△) open and (○) closed GDP reactors as a function of the CH_4/O_2 ratio. Experimental conditions are at OCV, 450 sccm and 700 °C. The 1 Hz and 1 kHz data points are marked with filled symbols.

indicates that the full-size cathode cell would have a mean temperature that is about 10–15 °C colder at a high CH_4/O_2 ratio than the small cathode cells when positioned in the center and at the outlet. This unexpected cooling effect is explained by the combustion processes that occur at the LSM cathode sintered at 1100 °C [11]. Indeed, on a full-size cathode, total methane oxidation is at its maximum level at the inlet where a fresh CH_4/O_2 gas mixture is allowed to enter the reactor. Further down the length of the fuel cell, the full-size cathode becomes less active due to a decreasing amount of CH_4/O_2 and its dilution with the reaction products. Conversely, the small cathodes positioned at the center and at the outlet are always exposed to the original CH_4/O_2 gas mixture. As a result, they are more reactive and the total combustion there leads to higher temperatures than on a full-size cathode at the same location. This heating effect in the coldest parts of the fuel cell also means that the use of small but active cathodes to measure the temperature variations along a full-size anode leads to a major underestimation of the temperature gradient downstream of the single chamber fuel cell inlet. To more precisely evaluate the temperature variation along the anode component, it is thus preferable to use completely

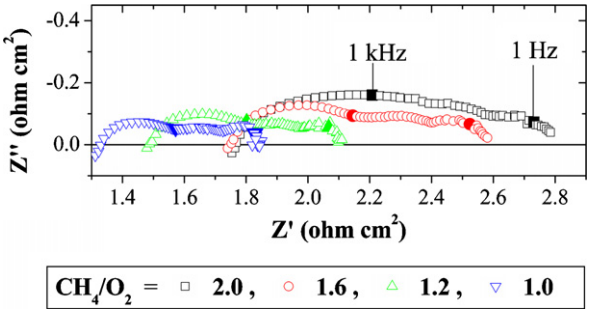

Fig. 6. Impedance spectra of the full-size Ni-YSZ/YSZ/LSM cell measured at OCV and 700 °C against various CH_4/O_2 ratios. Experiments performed in an open GDP reactor and 450 sccm total flow rate. The 1 Hz and 1 kHz data points are marked with filled symbols.

Table 2
Open circuit voltage of small cathode cells located at the inlet, center and outlet of identical electrolyte-supported half-cell anodes in either an open or closed GDP reactor.

CH_4/O_2	OCV (mV) (open GDP)			OCV (mV) (closed GDP)
	Inlet	Center	Outlet	Outlet
2.0	1,013	997	729	1,010
1.6	1,001	1,002	727	992
1.2	955	970	883	972
1.0	925	951	917	954

Furnace temperature is 700 °C and total flow rate is 450 sccm.

inactive cathode materials. Gold would certainly be the best material [24], but an LSM cathode sintered at a high enough temperature may also be appropriate if the operating temperature is not too high [11]. To this end, the catalytic activity of any cathode materials should be tested under real single chamber conditions.

In terms of total cell resistance, the $R_{t,cell}$ values of the full-size cathode closely mirror those at the center cathode at every CH_4/O_2 ratio (see Table 1). This is explained by the less pronounced effect that the oxygen depletion observed as a limiting process in the impedance spectra of the outlet cathode may have on the complete cell. Indeed, Fig. 6 still shows the presence of low frequency semi-circles in the full-size cathode spectra. However, they are much less predominant at high CH_4/O_2 ratios than for the spectra of the small outlet cathode cell (Fig. 3b). In fact, a full-size cathode levels off the impedance measured at the individual small cathode cells. This is in agreement with our previous observation [17], namely that the resistance of the full-size cathode cell is the sum of the individual inlet, center, and outlet cathode cells forming a parallel circuit.

3.3. Performances along single chamber SOFCs as a function of the CH_4/O_2 ratio (small and full-size cathodes)

Galvanodynamic cell discharge experiments under the same conditions of furnace temperature (700 °C) and total flow rates (450 sccm) were also performed for the four configurations of cells tested in the open GDP reactor. Standard *E–j* curves were obtained similar to those measured earlier at $CH_4/O_2 = 1.0$ [17]. Increasing the CH_4/O_2 ratio in all cases led to a general loss of maximum power density, P_{max}, as well as an important decrease in OCV for the cell made of a small cathode positioned at the outlet.

In terms of voltage variations first, Table 2 presents the OCV data of the small inlet, center and outlet cathode cells in the open GDP reactor that are compared to the second outlet cathode cell tested in the closed GDP reactor. In the open reactor, the inlet and center cathodes always show normal OCV values close to 1.0 V. The outlet cathode, however, displays major decreases with increasing CH_4/O_2. At $CH_4/O_2 \geq 1.6$, OCV reaches values of only about 0.73 V. Conversely, in the closed GDP reactor, an identical small outlet cathode cell always exhibits normal OCV values of about 0.95–1.0 V from $CH_4/O_2 = 1.0$–2.0. This marked difference in OCV between the outlet cathodes in the open and closed GDP supports the idea of accelerated lateral flow rates along the cell and of oxygen depletion at the most downstream position of the fuel cell. The use of gas distribution plates that confine the chemical environment above the electrodes favours maximum oxygen partial pressure over the cathode at any location downstream from the inlet gas mixture and restores normal cell voltage. Lastly, the full-size cathode tested in the open GDP reactor was affected to a certain extent by the presence of gas leakage. However, its OCV values were stable and relatively high (between 0.90 and 0.95 V).

In terms of performance, Fig. 7 shows the variations in P_{max} as a function of the CH_4/O_2 ratio for every cell tested in the open GDP reactor. In the range studied, the inlet cathode cell always

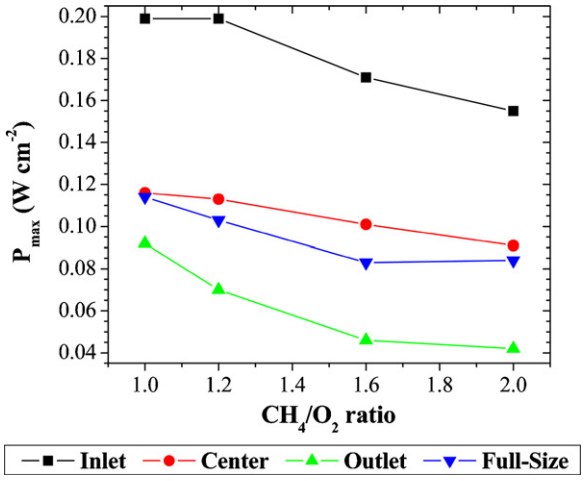

Fig. 7. Maximum power densities recorded for the three small cathode positions and for the full-size cathode cell as a function of the CH_4/O_2 ratio. Experiments performed in an open GDP reactor at 700 °C and 450 sccm total flow rate.

performs the best and the outlet cathode cell the worst. The full-size cathode cell has a performance that is close to the small center cathode. However, the actual results clearly show that performance is not uniform along this full-size cathode cell. On one hand, at $CH_4/O_2 = 2.0$, for example, the first third of the cell should have a mean P_{max} of about 155 mW cm^{-2} like the small inlet cathode cell. On the other hand, its last third should reach only about 40 mW cm^{-2}, the same as for the small outlet cathode cell. Overall, however, a mean P_{max} of 84 mW cm^{-2} is recorded close to the 91 mW cm^{-2} obtained on the center cathode cell.

P_{max} generally decreases with an increase in the CH_4/O_2 ratios and closely follows the calculated rise in temperature of the individual fuel cells (Fig. 4). The latter relationship between cell temperature and power densities was expected, however, since fuel cell performance should be controlled by the ohmic resistance of the thick YSZ electrolyte with our experimental conditions. The only exception to this rule is the outlet cathode cell. By increasing the CH_4/O_2 ratio, its temperature comes closer to the center cathode due to the use of an active LSM material for the combustion of CH_4 (see Section 3.2). One would thus expect the P_{max} values to approach those measured at the center cathode at the highest CH_4/O_2 ratios. However, its power densities are always the lowest and in fact rapidly move away from the center cathode in increasing the CH_4/O_2 ratio from 1.0 (Fig. 7). This discrepancy between the achieved cell temperature and the recorded P_{max} has to be caused by the more pronounced effect that oxygen depletion downstream of the cells tested in an open GDP reactor has on electrode polarization resistance. As seen before in our EIS measurements, the latter phenomenon induces an additional limiting process at low frequency, which increases as the CH_4/O_2 ratio rises (see Fig. 3). Under such conditions, the performance of the outlet cathode cell becomes dependent on total cell resistance and not only on actual cell temperature. A more normal dependency with the ohmic resistance of the electrolyte would have been probably found inside a closed GDP reactor.

Variations in P_{max} as a function of the CH_4/O_2 ratio have been studied before on similar though anode supported Ni-YSZ cells. Jacques-Bédard et al. [19] found a maximum value in P_{max} at about 1.5 in agreement with the maximum overheating value measured between 0.5 and 2.0. This ratio corresponds fairly well to the value of 1.67 calculated by Hao and Goodwin [20] using a two-dimensional numerical model. More recently, however, on a stack of two cells connected in series, Liu et al. [21] measured rising performances with a decrease in the CH_4/O_2 ratios between 2.0 and 1.0. Although in agreement with the present investigation, this better performance at $CH_4/O_2 = 1.0$ may be fortuitous due to differences in cell configuration and reactor design. Indeed, as mentioned by Hao and Goodwin [20], the optimum fuel-to-oxygen ratio is affected by the coupling of many physical and chemical processes like temperature, electrode catalyst activity, electrode microstructure, flow geometry, and exchange current density. However, clear discrepancies exist between the present study and the earlier work of Jacques-Bédard et al. [19] in spite of the very similar experimental conditions. The difference between both experiments essentially resides in the fuel cells themselves and more precisely in the thickness of the anode components; 50 μm in the actual electrolyte-supported cells as oppose to more than 500 μm in the anode supported cells. This strongly supports catalysis as the key factor involved in the two dissimilar behaviours observed here for the variations in P_{max} as a function of the CH_4/O_2 ratios. Increased amounts of Ni active sites and a longer diffusion path in the thick anode supported cells, for example, may give rise to different catalytic reaction mechanisms or new side reactions. More detailed catalytic studies as a function of electrode materials and operating conditions would be required to confirm the direct influence that heterogeneous catalysis may have on the optimum fuel-to-oxygen ratio in SC-SOFCs.

4. Conclusion

The use of small cathode cells and impedance spectroscopy for measuring the temperature along single chamber SOFCs yields misleading results if the cathode materials are active for the conversion of the hydrocarbon fuels. In such a case, they produce some unusual heating in the coldest part of the cells and an underestimation of the temperature gradients. This effect may be corrected by the use of gold or perovskite materials that are sintered at high enough temperatures.

Single chamber reactor design is especially important to lessen the performance gradient along SC-SOFCs. Open gas distribution plates allow extensive lateral flow rates and gas leakage away from the electrode surfaces. They lead to oxygen depletion and lower voltages downstream of the fuel cell inlet. As a result, they also induce additional low frequency semicircles in the EIS spectra recorded at the fuel cell outlet. These LF features rapidly expand with a decrease in the oxygen content of the fuel gas mixture. The use of closed gas distribution plates that confine the environment over the electrodes prevents such gas leakage and drops in performance.

The sustained combustion of methane in SC-SOFCs gives rise to sharp exothermic heating especially at the fuel cell inlet, and to a steep temperature gradient along its length. On an electrolyte-supported Ni-YSZ/YSZ/LSM cell, an increase in the CH_4/O_2 ratios between 1.0 and 2.0 results in a reduction of the heat released and, accordingly, of the performance. Maximum power density strongly depends on the size of the fuel cell, especially for single chamber reactors that include open gas distribution plates. The present investigation displayed reductions of about 50–75% of the mean P_{max} values between the inlet and the outlet of a 3.2 cm^2 cell measuring 23 mm lengthwise. Hence, the findings bring up the issue of the minimum fuel cell area in laboratory-scale SC-SOFCs experiments and of practical design to achieve the best possible gas distribution in single chamber reactors.

Acknowledgements

The authors thank the Natural Sciences and Engineering Research Council of Canada and Hydro-Québec for their financial support.

References

[1] T. Hibino, H. Tsunekawa, S. Tanimoto, M. Sano, Journal of the Electrochemical Society 147 (2000) 1338–1343.
[2] I.C. Stefan, C.P. Jacobson, S.J. Visco, L.C. De Jonghe, Electrochemical and Solid State Letters 7 (2004) A198–A200.
[3] T.W. Napporn, X. Jacques-Bédard, F. Morin, M. Meunier, Journal of the Electrochemical Society 151 (2004) A2088–A2094.
[4] B.E. Buergler, M.E. Siegrist, L.J. Gauckler, Solid State Ionics 176 (2005) 1717–1722.
[5] T. Suzuki, P. Jasinski, V. Petrovsky, H.U. Anderson, F. Dogan, Journal of the Electrochemical Society 152 (2005) A527–A531.
[6] M. Yano, A. Tomita, M. Sano, T. Hibino, Solid State Ionics 177 (2007) 3351–3359.
[7] I. Riess, Journal of Power Sources 175 (2008) 325–337.
[8] T. Suzuki, P. Jasinski, H.U. Anderson, F. Dogan, Journal of the Electrochemical Society 151 (2004) A1678–A1682.
[9] Z. Shao, C. Kwak, S.M. Haile, Solid State Ionics 175 (2004) 39–46.
[10] Z. Shao, S.M. Haile, Nature 431 (2004) 170–173.
[11] B. Morel, R. Roberge, S. Savoie, T.W. Napporn, M. Meunier, Applied Catalysis A: General 323 (2007) 181–187.
[12] T. Hibino, A. Hashimoto, T. Inoue, J.-I. Tokuno, S.-I. Yoshida, M. Sano, Journal of the Electrochemical Society 148 (2001) A544–A549.
[13] T.W. Napporn, F. Morin, M. Meunier, Electrochemical and Solid-State Letters 7 (2004) A60–A62.
[14] T. Suzuki, P. Jasinski, V. Petrovsky, H.U. Anderson, F. Dogan, Journal of the Electrochemical Society 151 (2004) A1473–A1476.
[15] Z. Shao, J. Mederos, W.C. Chueh, S.M. Haile, Journal of Power Sources 162 (2006) 589–596.
[16] Z.P. Shao, S.M. Haile, J. Ahn, P.D. Ronney, Z.L. Zhan, S.A. Barnett, Nature 435 (2005) 795–798.
[17] B. Morel, R. Roberge, S. Savoie, T.W. Napporn, M. Meunier, Electrochemical and Solid-State Letters 10 (2007) B31–B33.
[18] T. Hibino, A. Hashimoto, M. Yano, M. Suzuki, S.-i. Yoshida, M. Sanob, Journal of the Electrochemical Society 149 (2002) A133–A136.
[19] X. Jacques-Bédard, T.W. Napporn, R. Roberge, M. Meunier, Journal of Power Sources 153 (2006) 108–113.
[20] Y. Hao, D.G. Goodwin, Journal of the Electrochemical Society 154 (2007) B207–B212.
[21] M. Liu, Z. Lu, B. Wei, R. Zhu, X. Huang, K. Chen, G. Ai, W. Su, Journal of the Electrochemical Society 154 (2007) B588–B592.
[22] T. Hibino, S. Wang, S. Kakimoto, M. Sano, Electrochemical and Solid-State Letters 2 (1999) 317–319.
[23] Y.H. Hu, E. Ruckenstein, in: B.C. Gates, H. Knoezinger (Eds.), Advances in Catalysis, Academic Press, New York, 2004, pp. 297–345.
[24] A.K. Demin, F.Y. Gulbis, Solid State Ionics 135 (2000) 451–456.